A novel type of cellular senescence that can be enhanced in mouse models and human tumor xenografts to suppress prostate tumorigenesis

Andrea Alimonti,[1,2] Caterina Nardella,[1,2] Zhenbang Chen,[1,2] John G. Clohessy,[1,2] Arkaitz Carracedo,[1,2] Lloyd C. Trotman,[2] Ke Cheng,[1,2] Shohreh Varmeh,[1,2] Sara C. Kozma,[3] George Thomas,[3] Erika Rosivatz,[4] Rudiger Woscholski,[4] Francesco Cognetti,[5] Howard I. Scher,[6] and Pier Paolo Pandolfi[1,2]

[1]Cancer Genetics Program, Beth Israel Deaconess Cancer Center, Departments of Medicine and Pathology, Beth Israel Deaconess Medical Center, Harvard Medical School, Boston, Massachusetts. [2]Cancer Biology and Genetics Program and Department of Pathology, Sloan-Kettering Institute, Memorial Sloan-Kettering Cancer Center, New York, New York. [3]Department of Genome Science, Genome Research Institute, University of Cincinnati, Ohio. [4]Division of Cell and Molecular Biology, Imperial College London, United Kingdom. [5]Department of Oncology, Regina Elena Cancer Institute, Rome, Italy. [6]Department of Medicine, Sloan-Kettering Institute, Memorial Sloan-Kettering Cancer Center.

Irreversible cell growth arrest, a process termed cellular senescence, is emerging as an intrinsic tumor suppressive mechanism. Oncogene-induced senescence is thought to be invariably preceded by hyperproliferation, aberrant replication, and activation of a DNA damage checkpoint response (DDR), rendering therapeutic enhancement of this process unsuitable for cancer treatment. We previously demonstrated in a mouse model of prostate cancer that inactivation of the tumor suppressor phosphatase and tensin homolog deleted on chromosome 10 (Pten) elicits a senescence response that opposes tumorigenesis. Here, we show that Pten-loss–induced cellular senescence (PICS) represents a senescence response that is distinct from oncogene-induced senescence and can be targeted for cancer therapy. Using mouse embryonic fibroblasts, we determined that PICS occurs rapidly after Pten inactivation, in the absence of cellular proliferation and DDR. Further, we found that PICS is associated with enhanced p53 translation. Consistent with these data, we showed that in mice p53-stabilizing drugs potentiated PICS and its tumor suppressive potential. Importantly, we demonstrated that pharmacological inhibition of PTEN drives senescence and inhibits tumorigenesis in vivo in a human xenograft model of prostate cancer. Taken together, our data identify a type of cellular senescence that can be triggered in nonproliferating cells in the absence of DNA damage, which we believe will be useful for developing a "pro-senescence" approach for cancer prevention and therapy.

Introduction

Cellular senescence describes a terminal arrest of cell growth that is observed in response to various insults including an abnormally high activity of oncogenes (1). After its discovery and molecular characterization in vitro, it has only recently been recognized to specifically oppose tumor formation in various tissues in vivo, both in humans and in mice (2–6). This, together with the recent findings that senescence can also promote tumor clearance through the innate immune response (7), calls for the development of compounds targeting oncogenic pathways to drive senescence in cancer, which we refer to hereafter as "pro-senescence" therapy.

We have previously demonstrated that activation of the PI3K/AKT pathway achieved by complete loss of the tumor suppressor phosphatase and tensin homolog deleted on chromosome 10 (*PTEN*), induces a cellular senescence response, a process we here term *Pten*-loss–induced cellular senescence (PICS).

PTEN is one of the most frequently altered tumor suppressor genes in cancer and, in particular, prostate cancer (8–10). It catalyzes the conversion of the membrane lipid second messenger PIP3 to PIP2 and is therefore a key mediator of the AKT/PKB pathway (11, 12). Our studies have identified PTEN dosage as being critical in determining the mechanism by which prostate tumors evolve in vivo (13, 14). PTEN in the condition of heterozygosity can promote tumor initiation and proliferation (15). However, complete loss of PTEN can oppose prostate tumorigenesis by triggering a powerful p53-dependent cellular senescence response (3). This provides the most plausible explanation for why human prostate cancer at presentation does not select for complete loss of PTEN and highlights the role of PTEN haploinsufficiency for prostate cancer initiation (13). Importantly, PICS has also been recently demonstrated in primary human epithelial cells (16). Thus, compounds that enhance PICS would have great potential for pro-senescence therapy in cancer. This therapeutic approach could be particularly appealing in prostate cancer, in which an overwhelming majority of patients at presentation have lost one allele of PTEN while retaining an intact p53 response (17) and are therefore at the verge of the signalling outburst that would trigger cellular senescence upon loss or inhibition of the remaining PTEN allele.

However, a major conceptual hurdle in considering a pro-senescence approach for cancer prevention and therapy is that oncogene-induced senescence (OIS) is preceded by hyperproliferation and consequent accumulation of a DNA damage checkpoint response (DDR) (18–22). These characteristics render the thera-

Conflict of interest: The authors have declared that no conflict of interest exists.
Citation for this article: *J Clin Invest.* 2010;120(3):681–693. doi:10.1172/JCI40535.

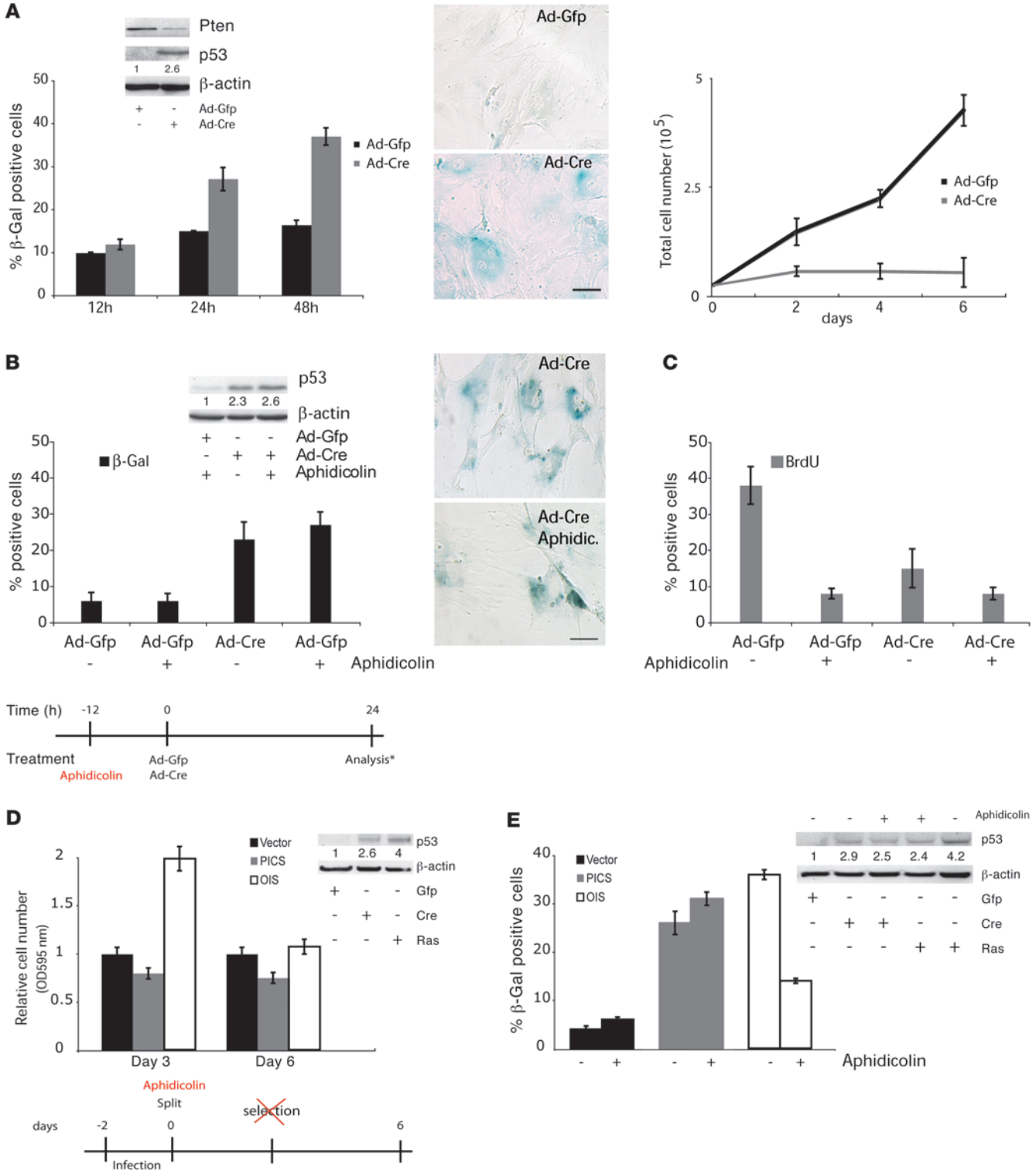
A
Pten
p53
β-actin
1 2.6
+ - Ad-Gfp
- + Ad-Cre
% β-Gal positive cells
Ad-Gfp
Ad-Cre
12h
24h
48h
Ad-Gfp
Ad-Cre
Total cell number (10^5)
days
B
p53
1 2.3 2.6
β-actin
Ad-Gfp
Ad-Cre
Aphidicolin
β-Gal
% positive cells
Ad-Cre
Ad-Cre Aphidic.
C
BrdU
% positive cells
Aphidicolin
Time (h) -12 0 24
Treatment
Aphidicolin
Ad-Gfp
Ad-Cre
Analysis*
D
Vector
PICS
OIS
p53
1 2.6 4
β-actin
Gfp
Cre
Ras
Relative cell number (OD595 nm)
Day 3
Day 6
Aphidicolin
Split
selection
days -2 0 6
Infection
E
Aphidicolin
p53
1 2.9 2.5 2.4 4.2
β-actin
Gfp
Cre
Ras
Vector
PICS
OIS
% β-Gal positive cells
Aphidicolin

Figure 1
Senescence driven by *Pten* loss occurs in the absence of cellular proliferation. (**A**) Western blot analysis of $Pten^{lx/lx}$ MEFs infected with Ad-GFP or Ad-Cre, according to the scheme in Supplemental Figure 1E. β-gal staining for senescence and its quantification. Scale bar: 10 μm. Growth curve of $Pten^{lx/lx}$ MEFs after infection with Ad-GFP or Ad-Cre. (**B**) Quantification of β-gal staining for senescence and Western blot analysis for p53 in $Pten^{lx/lx}$ MEFs treated according to the experimental timeline. The asterisk denotes analysis through either Western blotting or β-gal staining. Images show β-gal staining for senescence (at 24 hours). Scale bar: 10 μm. (**C**) Quantification of BrdU incorporation in $Pten^{lx/lx}$ MEFs infected as in **B**. (**D**) Analysis of cellular proliferation and Western blot analysis for p53 of $Pten^{lx/lx}$ primary MEFs infected with retroviral control vector, H-Ras (OIS), and Cre (PICS), as measured by relative cell number over a 6-day period, and followed without selection. Note that the absence of selection was required, since H-Ras induced hyperproliferation 2 days after the infection of MEFs (a shorter time point than that observed in human cell lines; ref. 18), and the selection phase masked this phenomenon. Experimental design for the experiment is shown in the lower panel. (**E**) Quantification of β-gal staining and Western blot analysis for p53 at day 6 for $Pten^{lx/lx}$ primary MEFs infected as in **D** (see experimental design in **D**). Numbers in the Western blots indicate densitometrically determined protein levels relative to β-actin (**A**, **B**, **D**, and **E**). Error bars show SD (**A**–**E**).

peutic enhancement of OIS unsuitable for cancer therapy. Hyperproliferation and DDR may promote the accumulation of arrested, albeit damaged, cells, favoring and not opposing cancer progression. Moreover, if hyperproliferation is indeed a prerequisite for the induction of cellular senescence, this would in turn limit a pro-senescence approach for the therapeutic targeting of proliferative cells, while sparing the quiescent cancer cell pool.

Although hyperproliferation and DDR have been proposed as the driving force in senescence induced by *Pten* loss (19), the molecular mechanisms that trigger senescence in response to acute inactivation of *Pten* are still poorly understood. Furthermore, the potential therapeutic application of targeting PICS in prostate cancer still remains unexplored.

Here, we identify PICS as a unique form of senescence that occurs in the absence of both DDR and hyper-replication. In addition to describing the features of this senescence response, we show that pharmacological modulation of this pathway may be effectively used as what we believe to be a novel therapeutic strategy and offer several examples of how to develop such an approach in vivo.

Results

PICS occurs in the absence of hyperproliferation. In characterizing PICS, we have discovered that upon complete inactivation of *Pten* in primary mouse embryonic fibroblasts (MEFs), the cells undergo senescence at early time points, without requiring a long-term hyperproliferative phase. As shown in Figure 1A, adenoviral-Cre (Ad-Cre) infection of primary *Pten* conditional knockout ($Pten^{lx/lx}$) MEFs efficiently reduced Pten protein (Figure 1A, inset) and gene levels (Supplemental Figure 1A; supplemental material available online with this article; doi:10.1172/JCI40535DS1) and resulted in induction of p53 protein level (Figure 1A, inset) and p21 transcription (Supplemental Figure 1B), consistent with our previous findings (3). Similarly, the hallmark feature of senescent cells, β-gal activity, revealed a rapid senescence response (Figure 1A) and a dramatic impairment in cell growth (Figure 1A). PICS was also associated with the increase of other well-characterized senescence markers, including p16 and PAI1 (3) (Supplemental Figure 1C).

Notably, acute inactivation of *Pten* by means of RNAi in *Pten* heterozygous ($Pten^{+/-}$) MEFs also resulted in induction of cellular senescence at early time points (Supplemental Figure 1D).

Since PICS occurred acutely and in the absence of a long-term hyperproliferative phase, we formed the hypothesis that PICS could occur in the complete absence of DNA replication and cellular proliferation, both characteristics of replicative senescence and OIS (18–22). To validate our hypothesis, we acutely inactivated *Pten* in MEFs pretreated with aphidicolin (see experimental timeline outlined in Figure 1), a reversible inhibitor of the eukaryotic DNA polymerase that specifically blocks the cell cycle at early S-phase by inhibiting DNA replication and that, as previously described, abrogates H-RAS–induced cellular senescence, the prototypic inducer of OIS (see below and ref. 5).

Pretreatment of $Pten^{lx/lx}$ MEFs with aphidicolin, followed by acute inactivation of *Pten*, resulted in increased β-gal senescence staining (Figure 1B) and p53 accumulation (Figure 1B) after 24 hours. This occurred in the absence of cellular proliferation, as visualized by the reduction of BrdU incorporation (Figure 1C), suggesting that in contrast to OIS DNA replication and cellular proliferation are not essential components of PICS.

To determine whether these represent genuine differences between PICS and OIS, we compared MEFs infected with $H\text{-}Ras^{V12}$ (H-Ras) and Cre for their ability to induce hyperproliferation prior to the induction of senescence. $Pten^{lx/lx}$ MEFs were infected with a retroviral vector containing activated H-Ras or Cre recombinase. Under these conditions, overexpression of H-Ras resulted in a consistent hyperproliferative phase, while infection with Cre resulted in decreased proliferation (Figure 1D). In addition, aphidicolin treatment of H-Ras–infected MEFs completely blunted the senescence response after the hyperproliferation in OIS (Figure 1E), partially preventing p53 accumulation (Figure 1E), while in contrast, the block of proliferation (Supplemental Figure 1F) did not affect PICS or p53 levels (Figure 1E). In sum, these data confirm that hyperproliferation is a prerequisite for OIS, which cannot be triggered in quiescent cells, while PICS can occur even in cells that are unable to proliferate.

PICS occurs independent of DNA damage. Since DNA hyper-replication drives senescence through the progressive accumulation of a DDR in OIS (18, 21, 22), we also looked for evidence of a DDR in MEFs that were progressively undergoing PICS and OIS. Control cells and cells undergoing PICS or OIS were followed for 96 hours with no apparent increase in senescence-associated DNA-damage foci (SDF) observed in PICS when compared with OIS (Figure 2A). SDF are characterized by immunofluorescent detection of the activated form of the ataxia telangiectasia protein (ATM pS1981) and activated DDR mediators such as phosphorylated histone H2AX (γ-H2AX) and phospho-p53 (Ser15) (Figure 2A). In addition cells undergoing OIS showed a significantly higher number of cells with large foci (Figure 2B and Supplemental Figure 2A for quantification) when compared with cells undergoing PICS and control. Western analysis was also carried out and did not show any increase in checkpoint kinase 1 (CHK1) phosphorylation on Ser345, CHK2 phosphorylation on Thr68, and phosphorylation of γ-H2AX, markers already shown to correlate with the DDR required for OIS (Figure 2C). In addition, a general increase in phosphorylation of ATM/ataxia telangiectasia (ATM/ATR) substrates (using anti–phospho-ST/Q) was not associated with PICS (Figure 2D), while the presence of DNA breaks in cells undergoing PICS, as detected by TUNEL, was also absent (Figure 2E).

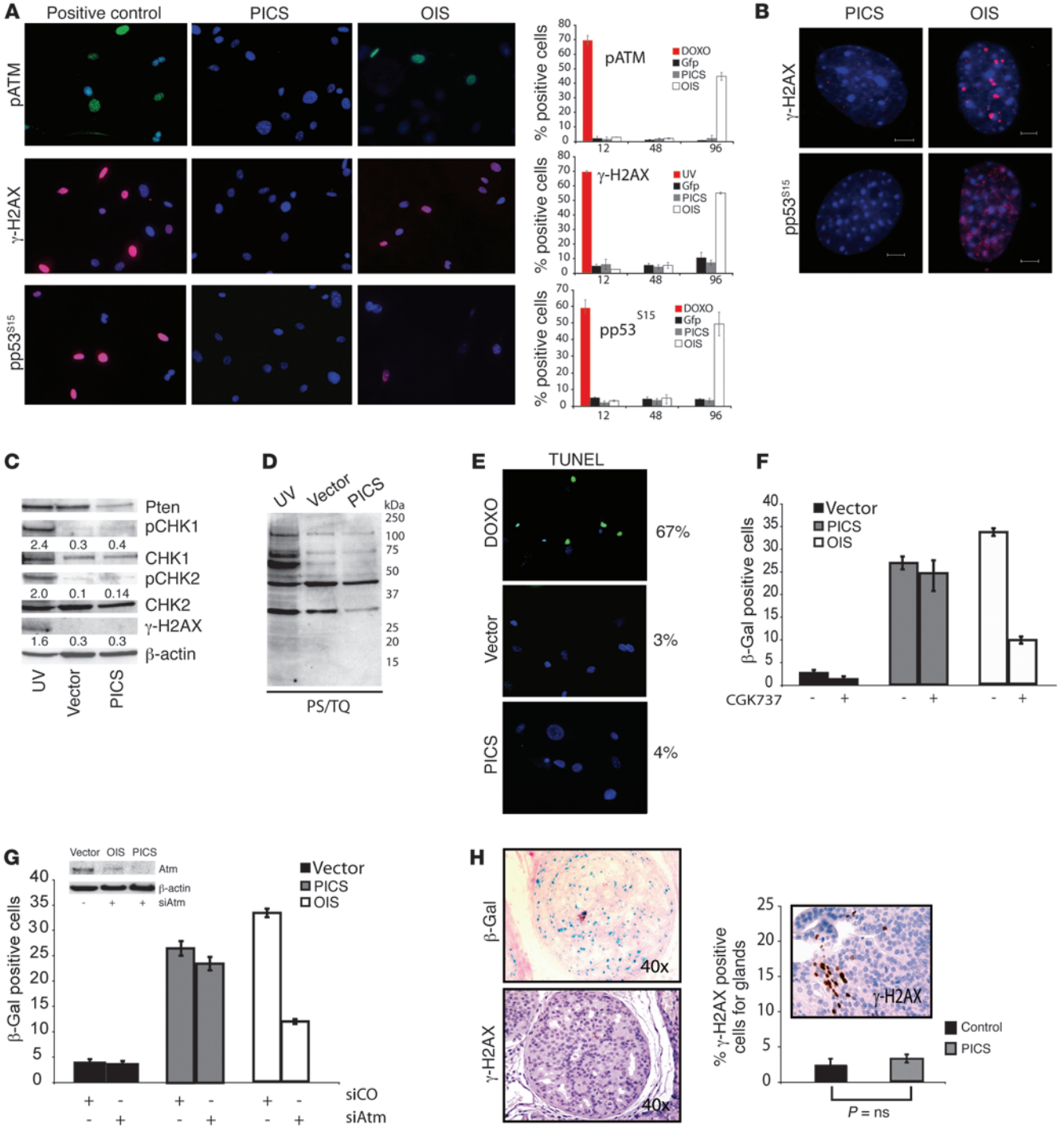
A
Positive control
PICS
OIS
pATM
γ-H2AX
pp53S15
% positive cells
pATM
DOXO
Gfp
PICS
OIS
γ-H2AX
UV
pp53S15
12
48
96
B
PICS
OIS
γ-H2AX
pp53S15
C
Pten
pCHK1
2.4 0.3 0.4
CHK1
pCHK2
2.0 0.1 0.14
CHK2
γ-H2AX
1.6 0.3 0.3
β-actin
UV
Vector
PICS
D
UV
Vector
PICS
kDa
250
100
75
50
37
25
20
15
PS/TQ
E
TUNEL
DOXO
67%
Vector
3%
PICS
4%
F
Vector
PICS
OIS
β-Gal positive cells
CGK737
- + - + - +
G
Vector OIS PICS
Atm
β-actin
siAtm
- + +
Vector
PICS
OIS
β-Gal positive cells
siCO
siAtm
H
β-Gal
40x
γ-H2AX
40x
% γ-H2AX positive cells for glands
γ-H2AX
Control
PICS
P = ns

Figure 2
Senescence driven by *Pten* loss occurs in the absence of DNA damage. (**A**) Immunofluorescence staining and its quantification to detect SDF in primary *Pten*$^{lx/lx}$ MEFs undergoing Cre (PICS) and H-Ras infection (OIS). Representative images of phospho-ATM (pATM), γ-H2AX, and phospho-p53 (Ser15) (pp53^{S15}) staining. MEFs treated with doxorubicin (DOXO) and UV were used as controls as indicated. (**B**) Representative images of γ-H2AX and phospho-p53 DNA damaged foci in MEFs treated as in **A**. Scale bar: 5 μm. (**C**) Western analysis for DDR markers in UV-treated primary WT MEFs, proliferating primary MEFs (vector), or MEFs undergoing PICS. Numbers in Western blots indicate protein levels for pCHK1, pCHK2, and γ-H2AX relative to β-actin. (**D**) Western analysis for substrates phosphorylated by ATM/ATR (phospho-S/TQ, PS/TQ) in UV-treated, control, and PICS. (**E**) TUNEL analysis in proliferating MEFs or MEFs undergoing PICS. WT MEFs treated with doxorubicin were used as a control. (**F**) Quantification of β-gal staining (at day 6) in *Pten*$^{lx/lx}$ MEFs infected as in **A** and treated with the ARM/ATR inhibitor CGK737 after infection. (**G**) Quantification of β-gal staining in MEFs infected as in **A** and transfected with either a control (siCO) or ATM-specific siRNA (siAtm). Western-blot analysis for ATM in MEFs infected and treated as indicated. (**H**) β-gal and phospho–γ-H2AX staining and its quantification in prostates from 8-week-old *Pten*$^{pc-/-}$ mice with prostatic intraepithelial neoplasia. The graph shows γ-H2AX staining in a positive control (a *Pten*$^{pc-/-}$ mouse with invasive carcinoma). *P* values were determined by Student's *t* test. Error bars show SD (**A** and **F**–**H**). Original magnification, ×10 (**A** and **E**); ×200 (inset in **H**).

DDR and p53 induction in OIS critically depend on the function of an intact ATM response (18, 19). We therefore tested whether p53 and a full-blown PICS response could be triggered in an ATM-independent manner. To this end, we used an RNAi approach to knockdown ATM in *Pten*$^{lx/lx}$ MEFs infected with Ad-Cre (Supplemental Figure 2B for the experimental timeline). Western analysis showed that at the time of infection with Ad-Cre, ATM levels were already significantly decreased (Supplemental Figure 2B, at 24 hours). Subsequent acute inactivation of *Pten* in these MEFs still resulted in the upregulation of p53 at early time points (Supplemental Figure 2C, at 72 hours). This allowed us to uncouple p53 induction from DDR activation and demonstrate that the establishment of DDR is not required for PICS.

To further validate our findings, H-Ras– and Cre-infected MEFs were treated with CGK733, a potent and selective small molecule inhibitor of the ATM/ATR kinase (23), and subsequently scored for senescence after treatment. Interestingly, CGK733 treatment completely inhibited H-Ras–induced senescence, while PICS remained unaffected (Figure 2F). Similarly, inactivation of ATM by RNAi resulted in decreased senescence in OIS but not in PICS (Figure 2G).

Finally, we analyzed samples from prostate conditional *Pten*-null mice (*Pten*$^{pc-/-}$), in which *Probasin-Cre* is used to conditionally inactivate *Pten* in the prostatic epithelium (3), for evidence of DDR activation in vivo. As previously reported, *Pten*$^{pc-/-}$ mice at the age of 8–11 weeks develop in situ prostate lesions [PIN]) that contain a significant number of β-gal–positive senescent cells, which also stain positive for p53 and p21 (at least 20-fold increase of the β-gal and p53 staining compared with WT prostates) (3). This powerful senescence response prevents tumor progression until its focal evasion, and at later stages, allows tumor invasion to occur (see below and ref. 3). Mice sacrificed at 8 weeks were stained for both β-gal and phospho–γ-H2AX. While we observed a strong senescence phenotype in the prostates of the *Pten*$^{pc-/-}$ mice, no significant difference in phospho–γ-H2AX was observed (Figure 2H, compare WT with early stage). Overall, our data support the hypothesis that when PICS is elicited the DDR is not engaged and that this senescence response is in fact independent of DDR activation.

Targeting PTEN for pro-senescence therapy in prostate cancer. The absence of such a DDR response, combined with our data demonstrating that PICS can be elicited in nonproliferating cells, renders the pharmacological targeting of PTEN appealing from a therapeutic point of view. This may be particularly relevant as conventional cytotoxic drugs do not efficiently target cells with low proliferative capacity and are relatively ineffective in quiescent cancer stem cells (24).

Thus, we reasoned that targeting upstream elements of the PI3K signaling pathway would represent a promising therapeutic strategy to trigger senescence in cancer cells, especially in cancer cells with low proliferative index. As partial reduction or monoallelic loss of *PTEN* is extremely frequent in human primary cancer (12) and in particular in prostate cancer, we tested whether transient and reversible pharmacological inhibition of Pten could trigger PICS. Note that a considerable number of prostate cancers often present with intact p53, even at late and metastatic stages of disease (25, 26). For instance some common cancer cell lines, such as LNCap and MDA PCa-2b, are derived from metastatic prostate cancer patients and yet maintain a functional p53 pathway (27).

To test the potential of this approach, we took advantage of a recently characterized PTEN inhibitor, VO-OHpic, developed as a potential anti-diabetes drug (28). VO-OHpic is a vanadyl complexed to hydroxypicolinic acid, which was recently found to be an inhibitor of PTEN, increasing cellular phosphatidylinositol-3,4,5-triphosphate (PIP3) levels, phosphorylation of AKT, and glucose uptake in adipocytes (28).

Treatment of WT and *Pten*$^{+/-}$ MEFs with vehicle or 500 nM VO-OHpic showed a clear, induction of senescence in *Pten*$^{+/-}$ cells, while WT control MEFs remained unaffected (Figure 3A). Importantly, proliferation of *Pten*$^{+/-}$ cells was impaired while WT cells were unaffected by VO-OHpic (Supplemental Figure 3A). This is in agreement with the fact that for senescence to be triggered *Pten* activity has to be significantly lowered below 50% and that only in cells with low basal levels of Pten can the inhibitor be effective. This in turn highlights the differential sensitivity of Pten mutant cells to VO-OHpic. Inhibition of Pten was confirmed by Western analysis, with both phospho-Akt (Ser473) and phospho-S6 levels increased in the *Pten*$^{+/-}$ treated cells (Figure 3B and Figure 3C for the quantification). *Pten* hypomorphic (*Pten*$^{hy/-}$) MEFs (30% of total protein level of Pten) were also treated with VO-OHpic, and although *Pten*$^{hy/-}$ MEFs had a higher background level of senescence to start with, VO-OHpic induced a significant increase in senescence also in these cells (Supplemental Figure 3B). Importantly, VO-OHpic did not induce further senescence in *Pten*$^{-/-}$ MEFs (Figure 3D).

We next checked whether treatment with VO-OHpic in human prostate cancer cell lines with reduced levels of PTEN and WT p53 could result in the induction of senescence. We first characterized 6 prostate cancer cell lines on the basis of PTEN and p53 levels (Figure 3E). In spite of the fact that these cell lines are derived from metastatic and advanced cancers, 3 were found to be WT for p53, with 1 cell line, MDA PCa-2b, expressing at the same time reduced levels of PTEN protein. On the basis of this genetic stratification,

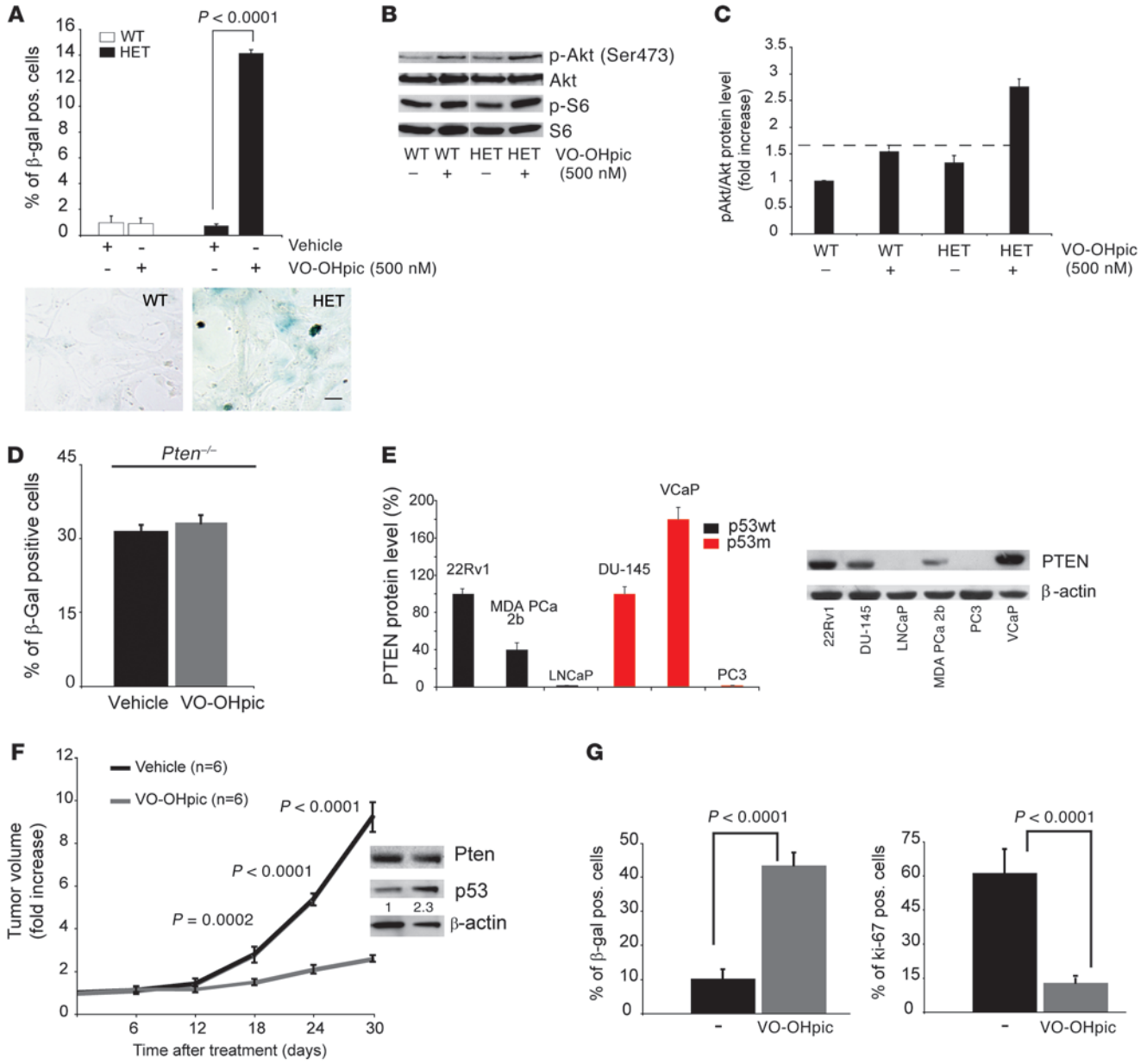

Figure 3

Pharmacological inhibition of PTEN drives senescence in vitro and in vivo. (**A**) Quantification of the senescence-associated β-gal assay and its staining in *Pten*$^{+/+}$ (WT) and *Pten*$^{+/-}$ (HET) cells treated with indicated concentrations of the PTEN inhibitor VO-OHpic. Scale bar: 10 μm. Error bars show SD. (**B**) Western analysis of cells from **A** treated with 500 nM VO-OHpic. Blot lanes were run on the same gel but were noncontiguous. (**C**) Quantification of pAkt (Ser 473)/Akt protein levels in *Pten*$^{+/+}$ and *Pten*$^{+/-}$ MEFs from **A**, normalized for the WT baseline level (dashed line). Error bars show SD from independent experiments. (**D**) Quantification of senescence-associated β-gal staining in *Pten*-null MEFs treated with either vehicle or 500 nM VO-OHpic. Error bars show SD. (**E**) Western analysis for PTEN and its quantification in 6 prostate cancer cell lines with WT (black bars) and mutant (red bars) p53. Error bars show SD from independent experiments. (**F**) Fold increase in tumor volume in a MDA PCa 2b xenograft mouse model after systemic treatment with VO-OHpic. Error bars show SD. A representative Western blot analysis for p53 in tumors from mice treated with Vehicle or VO-OHpic is shown in the inset. Numbers in the inset indicate densitometrically determined protein levels for p53 relative to β-actin (**G**) Quantification of β-gal– and Ki-67–positive cells in MDA PCa 2b tumors, untreated and treated with VO-OHpic. Error bars show SD. *P* indicates the statistical significance as measured by Student's *t* test throughout.

we studied the sensitivity of this cell line to PTEN inhibitors in vivo. Using MDA PCa-2b cells in a xenograft model, we observed a remarkable decrease in tumor growth when mice were treated systemically with VO-OHpic (Figure 3F). Notably, long-term treatment of MDA PCa-2b xenograft tumors with systemic VO-OHpic also resulted in an increased survival of the treated animals, due to the reduction of the tumor burden (data not shown). MDA PCa-2b tumors treated with VO-OHpic also presented an increased β-gal staining and a decreased Ki-67 staining when compared with the untreated control tumors (Figure 3G).

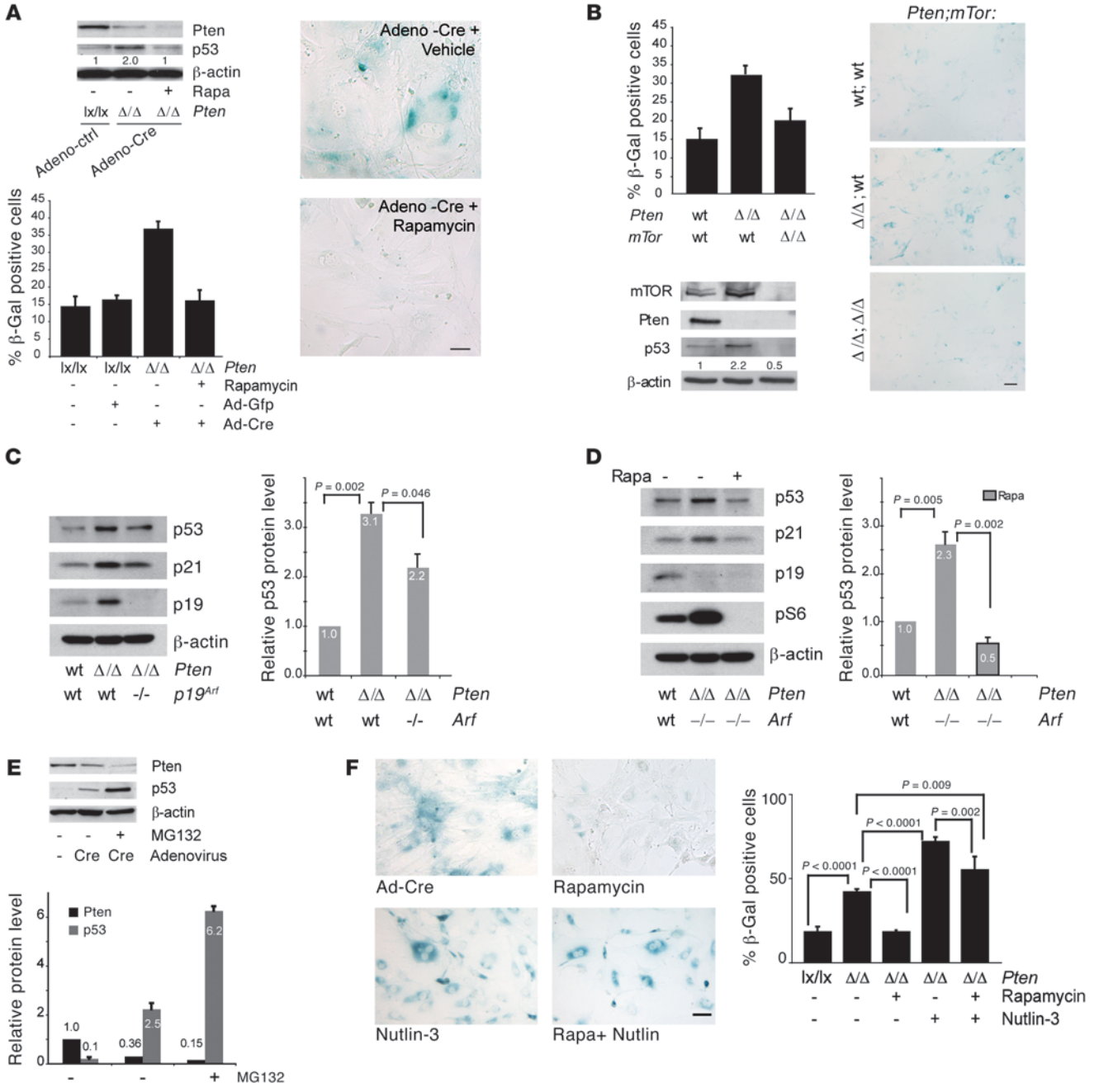

Figure 4

mTOR is essential for senescence upon Pten loss. (**A**) Western blot analysis of primary *Pten*$^{lx/lx}$ MEFs after rapamycin treatment and acute inactivation of Pten with Ad-Cre (Pten$^{\Delta/\Delta}$), according to the experimental scheme shown in Supplemental Figure 1E. Numbers indicate densitometrically determined protein levels relative to β-actin. Senescence-associated β-gal staining and its quantification is also shown. Scale bar: 10 μm. Error bars show SD. (**B**) Western analysis in Pten-deficient and Pten-mTOR compound mutant primary MEFs (by retroviral infection/selection). Numbers indicate densitometrically determined protein levels for p53 relative to β-actin. Senescence-associated β-gal staining and its quantification is also shown. Scale bar: 10 μm. Error bars show SD. (**C**) Western analysis of *Pten*$^{-/-}$*p19Arf*$^{-/-}$ compound mutant MEFs (by retroviral infection/selection) and quantification of p53 levels. Error bars show SD of 3 independent experiments. (**D**) MEFs as in **C**, treated with rapamycin (rapa) or DMSO for 24 hours. Error bars show SD of 3 independent experiments. (**E**) Western blot analysis and quantification for Pten and p53 protein levels of MEFs infected as in **A** and treated with MG132 48 hours after infection. Error bars show SD of 3 independent experiments. (**C**–**E**) Numbers within and above columns indicate the average p53 levels observed in independent experiments. (**F**) Senescence-associated β-gal staining and quantification of Pten$^{\Delta/\Delta}$ MEFs treated with rapamycin and/or Nutlin-3 during Ad-Cre–mediated PICS. Scale bar: 10 μm. Error bars show SD of 3 independent experiments. *P* indicates the statistical significance as measured by Student's *t* test throughout.

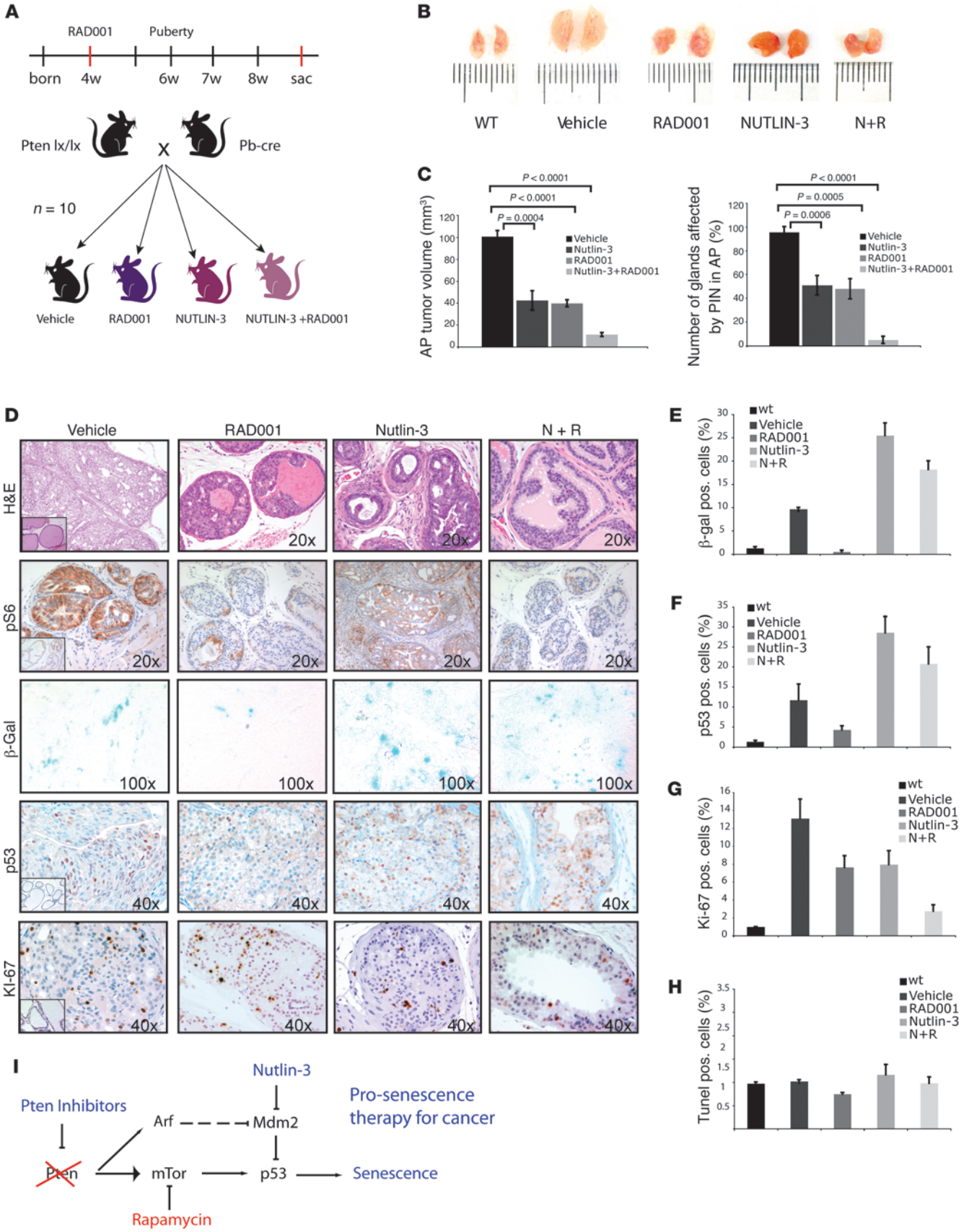
A
RAD001
Puberty
born
4w
6w
7w
8w
sac
Pten lx/lx
X
Pb-cre
n = 10
Vehicle
RAD001
NUTLIN-3
NUTLIN-3 +RAD001
B
WT
Vehicle
RAD001
NUTLIN-3
N+R
C
AP tumor volume (mm³)
P < 0.0001
P < 0.0001
P = 0.0004
Vehicle
Nutlin-3
RAD001
Nutlin-3+RAD001
Number of glands affected by PIN in AP (%)
P < 0.0001
P = 0.0005
P = 0.0006
D
Vehicle
RAD001
Nutlin-3
N + R
H&E
pS6
β-Gal
p53
KI-67
20x
100x
40x
E
β-gal pos. cells (%)
wt
Vehicle
RAD001
Nutlin-3
N+R
F
p53 pos. cells (%)
G
Ki-67 pos. cells (%)
H
Tunel pos. cells (%)
I
Nutlin-3
Pro-senescence therapy for cancer
Pten Inhibitors
Arf
Mdm2
Pten
mTor
p53
Senescence
Rapamycin

Figure 5
Nutlin-3 potentiates senescence and acts synergistically to RAD001 in restricting tumorigenesis in vivo. (**A**) Schematic representation of the timing of drug administration in the different treatment groups (n = 10 for each group). sac, sacrifice. (**B**) Sizes of the anterior prostate in $Pten^{pc-/-}$ mice (8 weeks of age) after the indicated treatments. (**C**) Quantification of the anterior prostates (APs) size and number of PIN-affected glands in mice (n = 6 for each treatment group) treated with the indicated drugs. Error bars show SD. P indicates the statistical significance (untreated versus each group of treatments). (**D**) Histopathological analysis and senescence of 8-week-old prostate tumors after treatments and staining as indicated: H&E, pS6, β-gal, p53, and Ki-67. Insets in H&E, pS6, p53, and Ki-67 represent a WT control stained as indicated (original magnification, ×20). (**E**) Quantification of the β-gal staining in anterior prostate sections of mice treated as indicate Representative sections from 3 mice were counted for each treatment group. Sections were counterstained with DAPI staining for β-gal quantification. (**F**) Quantification of p53 in the anterior prostate sections of mice treated as indicated. Sections from 3 mice were counted for each treatment group. (**G**) Quantification of Ki-67 staining in anterior prostates of mice treated as indicated and quantified as in **E**. (**H**) Quantification of TUNEL assay for apoptosis in the anterior prostates of mice treated as indicated (more than 3 mice per treatment group). Error bars in **E**–**H** represent SD for a representative experiment performed in triplicate. (**I**) Summary of the molecular pathway and pharmacological manipulation of PI3K pathway for pro-senescence therapy for cancer.

In sum, these findings demonstrate that treatment with PTEN inhibitors drives a tumor suppressive senescence response in a human prostate xenograft tumor. As PTEN inhibitors are already being proposed as potential drugs for treatment of other diseases, it is provocative to think that they may also be useful in the prevention and treatment of certain cancers.

PICS depends on mTOR function and is markedly potentiated by Mdm2 inhibition. Based on the above observations, we went on to characterized PICS in greater detail, and in doing so, we hypothesized that a downstream oncogenic component of the *Pten* pathway, when maximally activated, has the subversive ability to slow growth by inducing a senescence response that is independent of DDR activation. To test our hypothesis and to figure out which of the numerous targets of downstream *Pten* loss could be relevant, we tested the effect of rapamycin on PICS. Rapamycin, an antifungal macrolide with well-known immune-suppressive properties, inhibits the mTOR kinase complex 1 (mTORC1) (29). It is currently being tested for antitumoral activity in clinical trials (30) after several preclinical cancer model systems showed a response, especially under conditions of activated AKT/PKB signalling (31–33). mTOR is a key mediator of translation downstream of AKT through its ability to activate both initiation factor eIF4e as well as S6-kinase (29), and its functional activity has already been indirectly implicated in senescence in vivo (34, 35).

To test whether the senescence downstream of Akt activation depends on mTORC1, we treated primary $Pten^{lx/lx}$ MEFs with rapamycin prior to *Pten* ablation via infection with Ad-Cre (see Supplemental Figure 1E for a time line of the experiment). Surprisingly, while this procedure resulted in efficient *Pten* loss, senescence and p53 levels were completely abolished by rapamycin (Figure 4A). We also tested genetically whether mTOR is also essential for PICS, taking advantage of $Pten^{-/-}mTOR^{-/-}$ double-null MEFs, and found this to be true (Figure 4B).

As we have already established p53 to be a critical component of PICS in vivo (3), we set out to determine the relationship between mTOR and p53. Using real-time PCR we examined *Trp53* transcript levels between control and $Pten^{-/-}$ MEFs treated with either vehicle or rapamycin, and found there to be no difference (Supplemental Figure 4A). We therefore examined whether p53 upregulation observed in PICS could depend on a translational contribution of mTOR to this process. By pulsing cells undergoing PICS with [S^{35}]-labeled methionine we observed a significant proportion of newly synthesized p53 protein in cells undergoing PICS as compared with the control (Supplemental Figure 4B). Furthermore, the amount of *p53* mRNA loaded on the polysome, as analyzed by sucrose gradient, was higher in PICS (Supplemental Figure 4C) than in the control, while the amount of total *p53* mRNA remained unaffected. We also confirmed the relevance of our observations in vivo. To study the effect of pharmacological inhibition of mTOR in vivo, we used RAD001, a well-known analogue of rapamycin that has been previously tested in several prostate preclinical mouse models (30–32). In mice treated with RAD001, we observed a marked decrease in the total number of β-gal–positive cells and p53 staining as compared with control (Supplemental Figure 5).

Given the relevance of mTOR in PICS, our data suggested that the translational control of p53 in PICS may be dominant over Ink4a tumor suppressor gene product p19Arf–mediated (Arf-mediated) p53 stabilization. To determine the contribution of ARF in PICS, we genetically inactivated $p19^{Arf}$, and surprisingly, we observed that in a $Pten^{-/-}Arf^{-/-}$ background, neither the increase in p53 nor PICS were markedly reduced (ref. 36; Figure 4C and Supplemental Figure 6, A and B). Most notably, we found that the induction of p53 in $Pten^{-/-}Arf^{-/-}$ cells was completely rapamycin sensitive and hence mTOR dependent (Figure 4D). This is further supported by the finding that treatment with MG132 results in a substantial increase of p53 levels (Figure 4E, compare lane 2 with lane 3), in turn suggesting that the upregulation of Arf in PICS does not result in an effective transformed mouse 3T3 cell double minute 2 (Mdm2) blockade.

Thus, we reasoned that if Arf is not critical in opposing Mdm2 for the induction of p53 in PICS, perhaps the use of Mdm2 inhibitors, p53-stabilizing drugs such as Nutlin-3 (37), would lead to p53 superactivation and hence maximize the PICS response. As shown in Figure 4F, PICS was dramatically enhanced by treatment with Nutlin-3. Furthermore, Nutlin-3 could restore p53 levels and PICS even in cells pretreated with rapamycin (Figure 4F; see Supplemental Figure 1E for experimental scheme). The recovery of the PICS response was also accompanied by a strong p53-induction (Supplemental Figure 7A). Interestingly, WT MEFs treated simultaneously with Nutlin-3 and rapamycin were maximally growth inhibited when compared with the single administration of either drug (Supplemental Figure 7B), suggesting that the combination of both drugs can be effective in tumors that retain an intact p53 response. It is worth noting that the combination of the 2 drugs had no synergistic effect in $p53^{-/-}$ MEFs (Supplemental Figure 7B). Thus, p53-enhancing drugs, such as Nutlin-3, can be used to potentiate PICS for cancer chemoprevention and therapy. Notably, Nultin-3 was more effective in inducing senescence in PICS than in OIS (Supplemental Figure 7C). This can be explained by the major role played by $p19^{ARF}$ in OIS, which is already known to stabilize p53 through the inhibition of MDM2 (38). Finally no significant differences in term of senescence induction were observed in *Pten* WT and heterozygous MEFs (Supplemental Figure 7D) after treatment with Nutlin-3. On this basis, we hypothesized that Nutlins could be used as pow-

erful PICS enhancers and that mTOR inhibitors could be used in combination with Nutlins in order to take advantage of the pathway-inhibitory and pro-senescence activity of this drug combination, a hypothesis that we tested in vivo in preclinical trials.

Nutlin-3 potentiates PICS and synergizes with mTOR inhibition in vivo. We assessed whether Nutlin-3 would oppose *Pten*-loss–driven tumorigenesis by enhancing PICS in vivo singly or in combination with RAD001. Nutlin-3 was administered to $Pten^{pc-/-}$ mice at 4 weeks of age, prior to tumor onset (see Figure 5A for experimental scheme), and we scored for tumor size and number of PIN-affected glands.

Nutlin-3 decreased both the tumor size and the number of affected glands (Figure 5, B–D). This was associated with an increase of β-gal activity and p53 and p21 staining in all the glands analyzed (Figure 5, D–F, and Supplemental Figure 8). In contrast, although growth inhibitory, RAD001 markedly decreased senescence in almost all the remaining affected glands of the treated mice, as visualized by both a decrease in β-gal activity and p53 and p21 staining (Figure 5, D–F, and Supplemental Figure 8). The combination of Nutlin-3 and RAD001 rescued the senescence phenotype, as demonstrated by the increased tumors β-gal activity, p53 and p21 staining. The rescue of senescence resulted in a dramatic reduction of tumor size (Figure 5, B and C), number of affected glands (Figure 5C), and percentage of proliferating tumor cells (Figure 5, D and G). Notably, staining by TUNEL revealed no difference in apoptosis between the treatment groups, suggesting that the main function of Nutlin-3 in PICS is to enhance senescence rather than induce an apoptotic response (Figure 5H).

These findings validate the pro-senescence potential of Nutlin-3 in a genetically engineered mouse prostate model and represent a proof-of-principle example for the importance of the preservation of an intact senescence response in cancer chemoprevention and therapy. Our findings also suggest that treatment with mTOR inhibitors should be combined with drugs that sustain the p53 response. This is particularly relevant in prostate cancer, in which p53 function often remains intact (25, 26).

Discussion

For several years cellular senescence has been considered the result of replicative exhaustion of primary cells in vitro or the artifactual overexpression of oncogenes, with little evidence to prove the functional relevance of senescence in vivo. Recently, we and others have demonstrated that cellular senescence occurs in vivo and can oppose tumorigenesis in mouse models (2–5, 39). Specifically, our prostate mouse model has shown how potent the senescence response elicited by *Pten* loss is in restricting tumor initiation and progression (3). This finding has straightforward therapeutic implications for prostate cancer prevention and treatment and is especially relevant given that prostate cancer is still the most commonly diagnosed malignancy in men and the second most common cause of male cancer deaths (40). The recent discovery that senescence can drive tumor clearance trough the stimulation of a peritumoral immune response gives credence to the therapeutic application of pro-senescence compounds that can target senescence pathway for cancer therapy (16). Conventional chemotherapy and radiotherapy has been previously shown to induce cellular senescence in tumors samples of cancer patients but at the cost of cytotoxic effects for normal and cancer cells (41). Thus, it remained to be established whether the targeting of specific genes involved in senescence pathway (e.g., p53 or PTEN) could be used to induce senescence in vivo and whether this approach would efficiently oppose tumorigenesis. In this sense, targeted therapy oriented to modulate pro-senescence mediators could avoid the unselective genotoxicity delivered by conventional chemotherapeutics, thereby representing an alternative therapeutic strategy. Moreover, it was tempting to hypothesize that the genetic defects harbored by cancer cells (e.g., *Pten* heterozygous or homozygous loss) would render them differentially vulnerable to pro-senescence mediators. While our previous data regarding PICS clearly established an important role for the senescence response in opposing prostate tumorigenesis, it did not address the molecular and mechanistic details of the process. The new knowledge obtained in this study regarding the molecular and mechanistic requirements for PICS in turn offered important therapeutic opportunities that we could test both in vivo and in vitro.

Taken together, our findings lead to a number of relevant conclusions. First, we have characterized PICS as a novel form of cellular senescence, that unlike OIS does not trigger hyperproliferation and a classic DDR. These findings integrate the current notion whereby cellular senescence in response to some oncogenic stimuli would invariably represent, a checkpoint triggered by hyperproliferation, aberrant DNA replication, and DNA damage. These findings have therapeutic implications, since they suggest that compounds that enhance PICS by targeting PTEN or one of its downstream effectors will drive a beneficial senescence response without inducing DNA damage.

Second, we show that PICS can also be triggered in arrested cells and hence, in principle, be used to target for therapy even nonproliferating cells, including the quiescent cancer-initiating cell (24, 42). While the therapeutic enhancement of OIS would by definition spare the quiescent cell, in turn promoting the accumulation of arrested, albeit, damaged cells, therapeutic enhancement of PICS can be used to trigger the irreversible arrest of both proliferating and nonproliferating cells in the absence of DNA damage. Importantly, this also suggests that therapeutic delivery of DNA-damaging agents to cells undergoing PICS in the form, for instance, of ionizing radiation, could be used to further potentiate PICS or to morph this fail-safe response into full-blown apoptosis.

Third, we have further shown that a transient inhibition of PTEN can drive senescence in vivo in tumors with decreased PTEN protein levels. Given that current efforts in the fight against cancer aim at inhibiting PI3K-mTOR signalling, it is provocative to think that such PTEN inhibitors may represent a powerful class of molecules for pro-senescence therapy in *PTEN* heterozygous tumors and cells, keeping in mind that *PTEN* heterozygosity is commonly observed in human cancer (12).

Fourth, we have found that compounds that block mTOR can blunt senescence in tumors with activated senescence programs. Our unpublished observations also suggest that rapamycin and its analogues can antagonize the p53 response, upon treatment with ionizing radiation and chemotherapeutic agents. Thus, in addition to stabilization of p53, there can be a significant translational component to p53 upregulation in these conditions as well. Treatment with rapamycin specifically abrogates this upregulation and in doing so can blunt the p53 response so critical for opposing tumor progression. These undesired effects may limit the efficacy of rapamycin as a single agent in some instances.

Fifth, we have shown that the $Pten^{pc-/-}$ mouse model provides a unique setting to study the pro-senescence efficacy of novel and previously identify compounds alone or in combination. This in vivo approach has also allowed us to analyze the biological and genetic determinants of drug action in a manner that would be impossible using cell lines or in patients. Thus, this in vivo model has great potential for evaluating drug action and predicting treatment responses to pro-senescence therapeutic modalities.

Sixth, the elucidation of the molecular requirements underlying PICS has allowed us to identify a number of critical entry points for the rationale development of a pro-senescence therapy for cancer chemoprevention and treatment (Figure 5I). This will allow for an effective evaluation in the clinic of drugs that modulate PICS-inducing and PICS-suppressive pathways and for the development and fine tuning of protocols to improve efficacy and response to current treatments. This is exemplified by the case in hand, whereby inhibitors of p53 degradation, like Nutlin-3, can enhance senescence and overcome the negative effect of rapamycin and convert a rapamycin-mediated transitory growth arrest into terminal senescence. This approach could also prove very beneficial, as mTOR inhibition along with senescence induction could blunt at the same time the HIF-1α–mediated pro-angiogenic response, so critical for tumor progression (31).

Methods

Mouse crosses and MEF production. *mTOR* conditional knockout ($mTOR^{lx/lx}$; see ref. 43) mice were crossed with $Pten^{lx/lx}$ mice (see ref. 13) to produce $mTOR^{lx/lx}$-$Pten^{lx/lx}$ compound mutants (see reference for genotyping). MEFs from these crosses were harvested by standard procedures, and recombination was achieved as indicated below.

Cell culture, nude mice, treatments, and infection. Primary MEFs were transiently infected with Ad5-Cre (Microbix Biosystems Inc.) or with Ad5-GFP (gift of U. Greber and S. Hemmi, University of Zurich, Switzerland) for 48 hours at a multiplicity of infection of 50 as previously described (3). $Pten^{WT}$, $Pten^{+/-}$, $Pten^{Hypo/-}$ (30% of total dose of Pten protein), and $Pten^{-/-}$ primary MEFs were treated with varying doses of FBS (0.5%–20%). For stable transfections, primary MEFs ($Pten^{lx/lx}$, $mTOR^{lx//lx}$, and combinations including $p19^{Arf}$-null MEFs) were infected with retroviruses expressing Cre-PURO-IRES-GFP, Ras^{V12}-PURO-IRES-GFP, or control virus and selected in 3 μg/ml puromycin (Sigma-Aldrich) for 2 days as described (3) and used for analyses. For in vivo tumorigenesis assay, 5×10^6 cells of the indicated human prostate cancer cell lines were injected subcutaneously into the right flank of 6-week-old athymic nude mice (NCRNU-M; Taconic Farms Inc.). Animal experiments were approved by the Memorial Sloan-Kettering Cancer Center IACUC and Research Animal Resource Center of New York. RAD001 (everolimus, a derivative of rapamycin) was obtained from Novartis, and it was administered by oral gavage daily at 10^{-1} kg/d^{-1} for the indicated time. Nutlin-3 was obtained by Cayman Chemical (catalog 10004372) and was administered by intraperitoneal injection every other day at the dose of 100 mg/kg. Tumor size was measured using a 6-inch-dial caliper. Tumor volume was calculated according the following formula: $L \times W^2 \times 0.52$, where L indicates length and W indicates width. Infected MEFs were treated with 2 μg/ml aphidicolin (Sigma-Aldrich) and 20 nM rapamycin (Cell Signaling Technology) 12 hours prior to infection with Ad-Cre (see also experimental scheme in Supplemental Figure 1C) or 2 days after the infection with retroviral-Cre (see experimental scheme in Supplemental Figure 1D. The ATM/ATR inhibitor CGK737 (Sigma-Aldrich) was added at 1 μM (2 days after the infection with retroviral-Cre). Nutlin-3 (catalog 10004372; Cayman Chemical) was added at 10 μM and MG132 (Calbiochem) was used at 10 μM (see also experimental scheme in Supplemental Figure 1C), while the PTEN inhibitor VO-OHpic was used at concentrations up to 500 nM (28). For metabolic labeling, MEFs undergoing PICS were preincubated in DMEM without methionine and with cysteine and 5% dialyzed FBS for 1 hour. After starvation cells were labeled with 100 μCi/ml [^{35}S]-labeled methionine (Amersham) for 30 minutes. Cells were subsequently lysed, and immunoprecipitations for p53 were carried out as detailed below. Senescence staining was done using the Senescence Detection Kit (catalog JA7633; Calbiochem) as described (3), and quantifications were done on 4 images (roughly 500 cells) per experiment by determining the ratio of perinuclear blue–positive to perinuclear blue–negative cells. Growth curve analysis was also carried out as previously described (3). MEFs were treated with UV at the dose of 60 J/m^2 and Doxorubicin (Sigma-Aldrich) at the dose of 0.5 μM. TUNEL assays were performed with the In Situ Cell Death Detection kit (Roche), in accordance with the manufacturer's instructions; 50–100 cells were screened in each sample. The human prostate cancer cell lines, 22Rv1, MDA Pca 2b, LNCap, DU145, PC3, and VCaP and the human fibroblasts, WI-38, were obtained from ATCC.

Western blotting, immunoprecipitation, and immunochemistry. MEF lysates were prepared with RIPA buffer (1% PBS, 1% Nonidet P40, 0.5% sodium deoxycholate, 0.1% SDS and protease inhibitor cocktail; Roche). The following antibodies were used for Western blotting: mouse monoclonal anti-Pten (clone 6H2.1, catalog ABM-2052; Cascade BioScience), rabbit monoclonal anti-Pten (clone 138G6, catalog 9559; Cell Signaling Technology), rabbit polyclonal anti-$p19^{Arf}$ (Ab-1, catalog RB-1714-PO; Neomarkers), rabbit polyclonal anti-p53 (CM5, catalog NCL-p53-CM5p; Novocastra), rabbit polyclonal anti-Akt (catalog 9272; Cell Signaling Technology), anti–phospho-serine 473 of Akt (catalog 9271; Cell Signaling Technology), rabbit polyclonal anti–phospho-serine 240/244 of S6 (catalog 2217; Cell Signaling Technology), rabbit polyclonal anti-p21 (C-19, catalog sc-397; Santa Cruz Biotechnology), mouse monoclonal anti-actin (catalog AC-74; Sigma-Aldrich), anti–phospo-histone γ–H2AX (Ser139) (catalog 05-636; Upstate), rabbit polyclonal anti-mTOR (mTAb1, catalog 07-231; Upstate-Millipore), mouse monoclonal antibody to ATM (NB 100-220; Novus Biologicals), mouse monoclonal Chk1 (catalog 2360; Cell Signaling Technology), rabbit polyclonal phospho-Chk1 (ser 317) (catalog 2344; Cell Signaling Technology), rabbit polyclonal Chk2 (catalog 2662; Cell Signaling Technology), rabbit anti-Chk2, phospho (Thr68) polyclonal antibody (ab38461; Abcam), and phospho-ATM/ATR (Ser/Thr) substrate antibody (catalog 2851; Cell Signaling Technology). After standard SDS-PAGE and Western blotting techniques, proteins were visualized using the ECL system (Amersham Biosciences) and quantified using the ImageJ software (http://rsb.info.nih.gov/ij/) from NIH on Macintosh computers. Immunoprecipitation was carried out as previously described (44). Briefly, cells were scraped off a 10-cm dish with lysis buffer and incubated for 30 minutes at 4°C on a rocking platform. The 30-minute (17,949 *g*) supernatants were precleared with protein-G Sepharose beads (Amersham) for 1 hour, and mouse anti-p53 (1:1,000; catalog sc-100; Santa Cruz Biotechnology) was added to equal protein amounts of cleared supernatants for overnight incubation at 4°C, followed by protein-G Sepharose coprecipitation (1 hour) and 3 consecutive washes (5 minutes each) at 4°C with lysis buffer. For immunohistochemistry tissues were fixed in 10% formalin and embedded in paraffin blocks according to the standard procedures. The antibodies used to stain the sections for anti–phospho-histone (Ser139) γ-H2AX, anti-p53, and anti–phospho-serine 240/244 of S6 were the same as those used for Western blot analysis. Anti-p21 was from Santa Cruz Biotechnology (F-5); ki-67 was from Novocastra.

Immunofluorescence microscopy. Cells were fixed as previously described (44). Cover slips were mounted in anti-Fade (IMP) and sealed with clear nail polish. Confocal sections were obtained with a Leica DMRXA2 microscope (HCX PL APO 63× water objective, 1.2 nominal aperture) using

Leica Confocal Software version 2.61. Comparative immunofluorescence analyses were performed in parallel with identical acquisition parameters; 100–300 cells were screened for each antigen. All data analysis was done on Apple Macintosh Computers. The average size of γ-H2AX foci in 50 cells was also measured using the Leica Confocal Software version 2.61. The following antibodies were used for immunofluorescence: rabbit anti–phospho-histone (Ser139) γ-H2AX (catalog 2577; Cell Signaling Technology), phospho-p53 (Ser15) antibody (catalog 9284; Cell Signaling Technology), mouse anti–ATM-protein kinase pS1981 (catalog 200-301-400; Rockland), and mouse monoclonal anti-BrdU (catalog 555627; BD Biosciences).

Real-time and conventional PCR. Total RNA was extracted from the various MEFs after indicated treatments, using the TRIzol method (Invitrogen) and quantitative real-time PCR performed as described previously (44). Briefly, cDNA was produced from 2 μg RNA using the SuperScript III System (Invitrogen), using oligo dT primers, as suggested by the manufacturer. Quantitative real-time PCR was performed on a Roche LightCycler, using the Quantitect SYBR Green PCR Kit (Qiagen) and the following amplification protocol: 15 minutes at 95°C, 40 cycles (15 seconds at 94°C, 20 seconds at 57°C, 20 seconds at 72°C), followed by determination/confirmation of amplicon melting temperature. Reactions were performed in triplicates, primer pairs were confirmed to yield a single amplicon band by 3% agarose gel electrophoresis, and absence of amplification from non–reverse-transcribed RNA was confirmed to exclude genomic DNA amplification. The primer sequences were obtained from PrimerBank (http://pga.mgh.harvard.edu/primerbank/index.html) and have been described previously (45). Sequences used were as follows: p53 pair 1 (PrimerBank ID 6755881a1), forward 1 (5′-GCGTAAACGCTTCGAGATGTT-3′), reverse 1 (5′-TTTTTATGGCGGGAAGTAGACTG-3′); pair 2 (PrimerBank ID 6755881a2), forward 2 (5′-GATGCCCATGCTACAGAGGAG-3′), reverse 2 (5′TTTTTATGGCGGGAAGTAGACTG-3′); pair 3 (PrimerBank ID 6755881a3), forward 3 (5′-CTCTCCCCCGCAAAAGAAAAA-3′), reverse 3 (5′-CGGAACATCTCGAAGCGTTTA-3′). The following primers for Hprt1 and β-actin cDNA were used as reference standards: Hprt1, forward (5′-CACAGGACTAGAACACCTGC-3′), reverse (5′-GCTGGTGAAAAGGACCTCT-3′); β-actin, forward (5′-GGCCAACCGTGAAAAGATGA-3′), reverse (5′-TGGATGGCTACGTACATGGCT-3′).

Polysome fractionation. Polysome profiles were generated as previously described (46). Briefly, cytoplasmic cell extracts were sedimented on 10%–50% linear sucrose gradients by centrifugation at 156,500 *g* for 3 hours. Twelve fractions were collected from the gradients and monitored with an ISCO UA-6 detector. RNA was extracted from each fraction using the RNeasy Kit (Qiagen). Amplifications were run in a 7900 Real-Time PCR System (Applied Biosystems). The following TaqMan probes (Applied biosystems) were used for real-time PCR analysis: β2 microglobulin (Mm00437762_m1), HPRT1 (Mm00446968_m1), β-actin (Mm00607939_s1), and mouse p53 (Mm01731287_m1).

RNAi assays. MEFs were plated into 6-well dishes and transfected with anti-PTEN (SMARTpool; Dharmacon) and anti-ATM (SMARTpool; Dharmacon) siRNAs and control siRNA (si-Luc; Dharmacon), according to the manufacturer's instructions.

Statistics. Statistical evaluations were carried out using SigmaStat 2.03 (SPSS). For all tests, *P* values of less than 0.05 were considered significant.

Acknowledgments

We thank L. Poliseno, R. Bernardi, B. Carver, and L. Salmena for critical discussions, help with materials, and data analysis. This work was supported by NIH grants and the Prostate Cancer Foundation to P.P. Pandolfi. A. Alimonti was supported in part by a fellowship from Associazione Italiana di Oncologia Medica (AIOM) and S. Komen Cancer Foundations. C. Nardella was supported in part by a fellowship from the American Italian Cancer Foundation. A. Carracedo was supported by an EMBO long-term fellowship.

Received for publication July 16, 2009, and accepted in revised form December 16, 2009.

Address correspondence to: Pier Paolo Pandolfi, Cancer Genetics Program, Beth Israel Deaconess Cancer Center, Departments of Medicine and Pathology, Beth Israel Deaconess Medical Center, Harvard Medical School, 3 Blackfan Circle, CLS 401, Boston, MA 02115. Phone: 617.735.2121; Fax: 617.735.2120; E-mail: ppandolf@bidmc.harvard.edu.

1. Campisi J. Senescent cells, tumor suppression, and organismal aging: good citizens, bad neighbors. *Cell*. 2005;120(4):513–522.
2. Braig M, et al. Oncogene-induced senescence as an initial barrier in lymphoma development. *Nature*. 2005;436(7051):660–665.
3. Chen Z, et al. Crucial role of p53-dependent cellular senescence in suppression of Pten-deficient tumorigenesis. *Nature*. 2005;436(7051):725–730.
4. Collado M, et al. Tumour biology: senescence in premalignant tumours. *Nature*. 2005;436(7051):642.
5. Michaloglou C, et al. BRAFE600-associated senescence-like cell cycle arrest of human naevi. *Nature*. 2005;436(7051):720–724.
6. Campisi J. Suppressing cancer: the importance of being senescent. *Science*. 2005;309(5736):886–887.
7. Xue W, et al. Senescence and tumour clearance is triggered by p53 restoration in murine liver carcinomas. *Nature*. 2007;445(7128):656–660.
8. Li J, et al. PTEN, a putative protein tyrosine phosphatase gene mutated in human brain, breast, and prostate cancer. *Science*. 1997;275(5308):1943–1947.
9. Steck PA, et al. Identification of a candidate tumour suppressor gene, MMAC1, at chromosome 10q23.3 that is mutated in multiple advanced cancers. *Nat Genet*. 1997;15(4):356–362.
10. Teng DH, et al. MMAC1/PTEN mutations in primary tumor specimens and tumor cell lines. *Cancer Res*. 1997;57(23):5221–5225.
11. Stambolic V, et al. Negative regulation of PKB/Akt-dependent cell survival by the tumor suppressor PTEN. *Cell*. 1998;95(1):29–39.
12. Maehama T, Dixon JE. The tumor suppressor, PTEN/MMAC1, dephosphorylates the lipid second messenger, phosphatidylinositol 3,4,5-trisphosphate. *J Biol Chem*. 1998;273(22):13375–13378.
13. Trotman LC, et al. Pten dose dictates cancer progression in the prostate. *PLoS Biol*. 2003;1(3):E59.
14. Di Cristofano A, De Acetis M, Koff A, Cordon-Cardo C, Pandolfi PP. Pten and p27KIP1 cooperate in prostate cancer tumor suppression in the mouse. *Nat Genet*. 2001;27(2):222–224.
15. Di Cristofano A, Pesce B, Cordon-Cardo C, Pandolfi PP. Pten is essential for embryonic development and tumour suppression. *Nat Genet*. 1998;19(4):348–355.
16. Kim JS, Lee C, Bonifant CL, Ressom H, Waldman T. Activation of p53-dependent growth suppression in human cells by mutations in PTEN or PIK3CA. *Mol Cell Biol*. 2007;27(2):662–677.
17. Schlomm T, et al. Clinical significance of p53 alterations in surgically treated prostate cancers. *Mod Pathol*. 2008;21(11):1371–1378.
18. Di Micco R, et al. Oncogene-induced senescence is a DNA damage response triggered by DNA hyper-replication. *Nature*. 2006;444(7119):638–642.
19. Di Micco R, Fumagalli M, di Fagagna F. Breaking news: high-speed race ends in arrest--how oncogenes induce senescence. *Trends Cell Biol*. 2007;17(11):529–536.
20. Bartkova J, et al. DNA damage response as a candidate anti-cancer barrier in early human tumorigenesis. *Nature*. 2005;434(7035):864–870.
21. Bartkova J, et al. Oncogene-induced senescence is part of the tumorigenesis barrier imposed by DNA damage checkpoints. *Nature*. 2006;444(7119):633–637.
22. Mallette FA, Gaumont-Leclerc MF, Ferbeyre G. The DNA damage signaling pathway is a critical mediator of oncogene-induced senescence. *Genes Dev*. 2007;21(1):43–48.
23. Won J, et al. Small molecule-based reversible reprogramming of cellular lifespan. *Nat Chem Biol*. 2006;2(7):369–374.
24. Visvader JE, Lindeman GJ. Cancer stem cells in solid tumours: accumulating evidence and unresolved questions. *Nat Rev Cancer*. 2008;8(10):755–768.
25. Bookstein R, MacGrogan D, Hilsenbeck SG, Sharkey F, Allred DC. p53 is mutated in a subset of advanced-stage prostate cancers. *Cancer Res*. 1993;53(14):3369–3373.
26. Agell L, et al. KLF6 and TP53 mutations are a rare event in prostate cancer: distinguishing between Taq polymerase artifacts and true mutations. *Mod Pathol*. 2008;21(12):1470–1478.
27. Martinez LA, et al. p21 modulates threshold of apoptosis induced by DNA-damage and growth factor withdrawal in prostate cancer cells. *Carcinogenesis*. 2002;23(8):1289–1296.

28. Rosivatz E, et al. A small molecule inhibitor for phosphatase and tensin homologue deleted on chromosome 10 (PTEN). *ACS Chem Biol*. 2006;1(12):780–790.
29. Sabatini DM. mTOR and cancer: insights into a complex relationship. *Nat Rev Cancer*. 2006;6(9):729–734.
30. Thomas GV. mTOR and cancer: reason for dancing at the crossroads? *Curr Opin Genet Dev*. 2006;16(1):78–84.
31. Majumder PK, et al. mTOR inhibition reverses Akt-dependent prostate intraepithelial neoplasia through regulation of apoptotic and HIF-1-dependent pathways. *Nat Med*. 2004;10(6):594–601.
32. Neshat MS, et al. Enhanced sensitivity of PTEN-deficient tumors to inhibition of FRAP/mTOR. *Proc Natl Acad Sci U S A*. 2001;98(18):10314–10319.
33. Podsypanina K, et al. An inhibitor of mTOR reduces neoplasia and normalizes p70/S6 kinase activity in Pten+/– mice. *Proc Natl Acad Sci U S A*. 2001;98(18):10320–10325.
34. Ruggero D, et al. The translation factor eIF-4E promotes tumor formation and cooperates with c-Myc in lymphomagenesis. *Nat Med*. 2004;10(5):484–486.
35. Wendel HG, et al. Survival signalling by Akt and eIF4E in oncogenesis and cancer therapy. *Nature*. 2004;428(6980):332–337.
36. Chen Z, et al. Differential p53-independent outcomes of p19(Arf) loss in oncogenesis. *Sci Signal*. 2009;2(84):ra44.
37. Vassilev LT, et al. In vivo activation of the p53 pathway by small-molecule antagonists of MDM2. *Science*. 2004;303(5659):844–848.
38. Palmero I, Pantoja C, Serrano M. p19ARF links the tumour suppressor p53 to Ras. *Nature*. 1998;395(6698):125–126.
39. Sarkisian CJ, Keister BA, Stairs DB, Boxer RB, Moody SE, Chodosh LA. Dose-dependent oncogene-induced senescence in vivo and its evasion during mammary tumorigenesis. *Nat Cell Biol*. 2007;9(5):493–505.
40. Jemal A, Siegel R, Ward E, Murray T, Xu J, Thun MJ. Cancer statistics, 2007. *CA Cancer J Clin*. 2007;57(1):43–66.
41. Roninson IB. Tumor cell senescence in cancer treatment. *Cancer Res*. 2003;63(11):2705–2715.
42. Dean M, Fojo T, Bates S. Tumour stem cells and drug resistance. *Nat Rev Cancer*. 2005;5(4):275–284.
43. Gangloff YG, et al. Disruption of the mouse mTOR gene leads to early postimplantation lethality and prohibits embryonic stem cell development. *Mol Cell Biol*. 2004;24(21):9508–9516.
44. Trotman LC, et al. Identification of a tumour suppressor network opposing nuclear Akt function. *Nature*. 2006;441(7092):523–527.
45. Wang X, Seed B. A PCR primer bank for quantitative gene expression analysis. *Nucleic Acids Res*. 2003;31(24):e154.
46. Arava Y. Isolation of polysomal RNA for microarray analysis. *Methods Mol Biol*. 2003;224:79–87.